THE JOURNAL OF PHYSICAL CHEMISTRY Letters

Letter

pubs.acs.org/JPCL

Effective Mass-Driven Structural Transition in a Mn-Doped ZnS Nanoplatelet

Celine Gerard,[†,§] Ruma Das,[‡,§] Priya Mahadevan,*[,‡] and D. D. Sarma*[,†,∥]

[†]Solid State and Structural Chemistry Unit, Indian Institute of Science, Bangalore 560012, India

[‡]Department of Condensed Matter Physics and Material Sciences, S. N. Bose National Center for Basic Sciences, JD Block, Sector III, Salt Lake, Kolkata-700098, India

[∥]Council of Scientific and Industrial Research-Network of Institutes for Solar Energy (CSIR-NISE), New-Delhi, India

ABSTRACT: Mn doping in ZnS nanoplatelets has been shown to induce a structural transition from the wurtzite to the zinc blende phase. We trace the origin of this transition to quantum confinement effects, which shift the valence band maximum of the wurtzite and zinc blende polymorphs of ZnS at different rates as a function of the nanocrystal size, arising from different effective hole masses in the two structures. This modifies the covalency associated with Mn incorporation and is reflected in the size-dependent binding energy difference for the two structures.

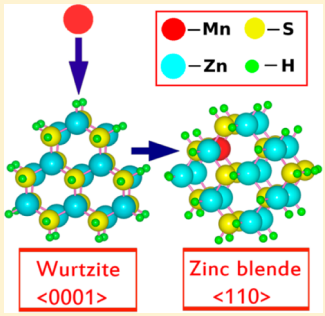

SECTION: Physical Processes in Nanomaterials and Nanostructures

Among binary semiconductors, formed by elements of the III−V and II−VI groups, one finds that the more ionic members favor the wurtzite structure, while the covalent ones are found to favor the zinc blende form,[1] with the other form (zinc blende and wurtzite, respectively) being available as a metastable state with an energy only a few meV per atom higher than the ground state.[2] Because physical and chemical properties of any material depend critically on the specific crystal structure, such a low-lying metastable state holds out the interesting possibility of tilting the energy balance in favor of the metastable phase even under small perturbations, thereby drastically altering material properties. The strong interplay between the structure of binary semiconductors and its consequential properties has been actively investigated for bulk materials over several decades now, using external parameters such as pressure and temperature.[3] At the nano regime, the large surface to volume ratio provides additional control parameters that have been effectively used in recent times to tune the structure of such binary semiconductor nanocrystals; such crystal structure transformations have been achieved by tuning growth conditions,[4] the choice of surface ligands,[5,6] or even just the size of the nanoparticles.[7] These results are easily understood in terms of the large contribution of the surface energy to the total energy of a nanoparticle in the small size regime. For example, the binding energy of a ligand attachment on the surface of a nanoparticle can be significantly different depending on its crystal structure;[5] thus, attaching ligands to most of the surface sites can significantly alter the total energy of a nanoparticle depending on its structure. Interestingly, there has been a recent report of a different class of structural transitions, namely reversible structural transformation of ZnS nanoplatelets that cannot be understood in terms of such relatively simple energy considerations because, among other reasons, it is reported to be triggered by the smallest level of reversible doping of Mn in the host.[8] We summarize below the essential and striking aspects of the experimental observations reported in ref 8.

It is found[8] that different sizes of the undoped ZnS nanoplatelets could be formed under certain synthesis conditions of carrying out the reaction in a solvent at an elevated temperature of 300 °C. These nanoplatelets invariably formed in the wurtzite structure independent of any subsequent temperature cycling of the reaction mixture or of the extracted nanocrystals redispersed in the solvent. Surprisingly, however, in the presence of a low concentration of Mn^{2+} ions in the solvent with redispersed ZnS nanoplatelets, it was found that the ZnS nanoplatelets transformed to the zinc blende structure at an elevated temperature of the solvent (>180 °C) accompanied by the insertion of Mn^{2+} ions into the host ZnS matrix, as evidenced from the appearance of the characteristic intense Mn^{2+} photoluminescence emission upon exciting the ZnS host and from electron paramagnetic resonance (EPR) studies.[8] Curiously, this transformation is found to be reversible with respect to a cycling of the temperature, with Mn^{2+} ions being ejected from the host ZnS nanoplatelet and the crystal structure of the host reverting back to the wurtzite one upon lowering the temperature below 180 °C. It is also reported in ref 8 that similar effects were not observed either for spherical

Received: February 6, 2013
Accepted: March 6, 2013
Published: March 6, 2013

   dx.doi.org/10.1021/jz4002746 | *J. Phys. Chem. Lett.* 2013, 4, 1023−1027

ZnS nanoparticles or ZnS nanoplatelets with sizes larger than 14 nm in diameter.

It is to be noted that there was no evidence of stacking faults in these nanocrystals in either of the two crystallographic forms, though transformations between wurtzite and zinc blende structures are known[9] to be usually driven by such stacking faults. Though a wurtzite to zinc blende transformation involving carrier doping has been suggested on the basis of theoretical investigations in certain bulk semiconductors,[10,11] such a mechanism cannot be invoked here because Mn^{2+} ions substitute the Zn ions isovalently without involving any carrier doping. In order to understand the microscopic origin of such an unusual phase transformation, we use first-principles electronic structure calculations carried out within the framework of density functional theory. Our results show that at a fundamental level, quantum confinement effects at the nanoscale are responsible for the observed phenomenon, the two structure types being discriminated by Mn incorporation/ejection essentially due to significantly different hole effective masses in the zinc blende and wurtzite phases. Our results also explain the absence of any such structural transformation above a certain size of the nanocrystal.

Nanoplatelets are constructed in the present investigation in accordance with the experimental observations[8] as follows: The growth direction for the wurtzite nanoplatelet has been taken as ⟨0001⟩, as observed experimentally, while both directions ⟨110⟩ and ⟨111⟩ were studied for the zinc blende nanoplatelet. Two different nanoplatelets with diameters of 0.75 and 1.5 nm have been investigated in the present study; both of these platelets have four monolayer thickness. The results are compared with corresponding results for the bulk. The bulk lattice constants of a = 5.41 Å for the zinc blende case[12] as well as a = 3.82 Å and c = 6.24 Å for the wurtzite case[12] were used for constructing the supercells corresponding to nanoplatelets of a given size. Along the x, y, and z directions, 12 Å of vacuum was used to ensure negligible interactions between the supercell units. We used projected augmented wave potentials[13] within a plane wave pseudopotential implementation of density functional theory in VASP code[14] with the LDA approximation[15] for the exchange–correlation functional. A plane wave cutoff energy for the basis sets of 280 eV has been used for the electronic structure calculations, which were performed at the Gamma point only. Besides two different sized nanoplatelets for each structure type and two differently oriented platelets for the zinc blende, we had to carry out a large number of calculations for each such constructed nanoplatelet, placing a Mn^{2+} ion at each of the nonequivalent Zn^{2+} sites to study the impact of Mn incorporation in these nanoplatelets. However, we have not attempted calculations with multiple Zn sites being simultaneously replaced by Mn ions because experimental findings indicated[8] that even a very dilute presence of Mn is sufficient to cause the structural transformation; moreover, the number of symmetry-inequivalent positions for incorporating even two Mn ions in a given nanoplatelet will make the number of calculations hopelessly large. It is to be noted that a complete optimization of all internal coordinates within the supercell for every doped and undoped nanoplatelet was carried out until the force on each atom was less than 0.05 eV/Å. As usual, the surface Zn and S atoms were passivated with pseudohydrogens. Spheres of radii 1 Å were constructed about each atom to calculate the atom and orbital-projected density of states.

We first calculated the formation energy of nanoplatelets as well as that for bulk ZnS in the two crystallographic forms. Calculated results are found to be in agreement with experimental observations. For example, the nanoplatelet of 0.75 nm diameter was found to be the most stable in the wurtzite form compared to that in the zinc blende form by about 100–200 meV per atom depending on the specific orientation (⟨110⟩ or ⟨111⟩) of the zinc blende nanoplatelets. In contrast, the zinc blende structure was found to be slightly (by ∼3 meV per atom) stabler compared to the wurtzite structure for the bulk ZnS, thus establishing a structural transition as a function of size for ZnS. With the correct structure predicted for the undoped nanoplatelets, we probe the implication of doping Mn in these systems. We note that the formation energy for one Mn incorporation is given by E_c(ZnS/Mn) − E_c(ZnS) − μ_{Zn} + μ_{Mn}, where μ's are the chemical potentials for the corresponding atoms and E_c(ZnS/Mn) and E_c(ZnS) are the total energies of the nanoplatelets with and without Mn doping in a given crystal structure, indicated by the subscript c; we use c = w or z to denote the wurtzite or the zinc blende structures, respectively. Because μ_{Zn} and μ_S refer to the element and, therefore, are independent of the structure, it suffices to compare the relative binding energy, defined as $\Delta E_c = E_c$(ZnS/Mn) − E_c(ZnS), for different crystal structures and orientations in order to understand the relative stabilities of different forms of nanoplatelets. In order to obtain important insights in the reactivity in each case, we also analyze the wave function corresponding to the valence band maximum (VBM) or the highest occupied molecular orbital. In the absence of a common reference frame, the energy position of the VBM for each case has been determined by referencing its energy to the averaged electrostatic potential associated with the central atom calculated assuming a unit charge within a sphere of radius 1 Å.

At the surface of these nanoplatelets, Zn sites are coordinated to either one or two pseudohydrogens. Evaluating the binding energy of Mn doping on the surface of the ZnS nanocrystals, we find that Mn is much more likely to attach itself at a site that has only one pseudohydrogen and three sulfur bonds independent of the structure or the growth direction. In order to understand the mechanism of Mn incorporation in the experimentally observed zinc blende ⟨110⟩ oriented nanoplatelets, we have evaluated the relative binding energy of Mn doping at different surface sites. The dopant sites for the 1.5 nm sized nanoplatelet are shown in Figure 1. Our results show that the relative binding energy is the highest for Mn incorporation at a near-edge position. This would suggest that the Mn

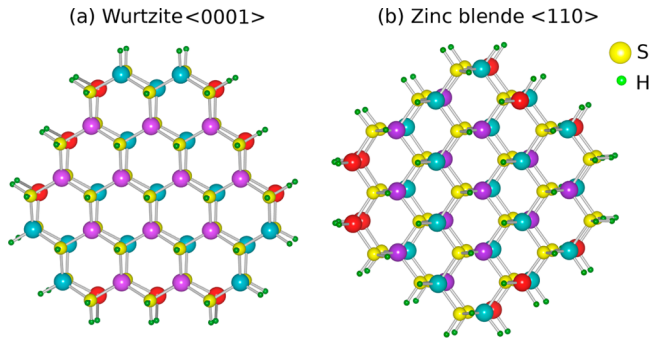

Figure 1. (a) Wurtzite ⟨0001⟩ and (b) zinc blende ⟨110⟩ ZnS nanoplatelets of medium size. Magenta, cyan, and red atoms are the Zn atoms which are 0-, 1-, and 2-fold coordinated with pseudohydrogens.

dx.doi.org/10.1021/jz4002746 | J. Phys. Chem. Lett. 2013, 4, 1023–1027

incorporation in ZnS nanoplatelets may begin with the incorporation of Mn at a near-edge site as the preferred site. This finds experimental support in the observation that the Mn-doping-induced phase transformation begins near the edge of the nanocrystal, as evidenced by transmission electron micrograph of nanoplatelets with arrested, incomplete structural transformation reported in ref 8. However, experimental evidence points to eventual incorporation of the Mn ion into a subsurface tetrahedrally coordinated site in the ground state, as deduced on the basis of EPR results.[8] In order to understand this result specifically and the relative binding energy of Mn at various sites of different nanoplatelets in general, we have carried out a large number of calculations with Mn at different inequivalent sites of the different nanoplatelets. We have tabulated the largest binding energy found in each size, namely, the small and medium nanoplatelets and the bulk, for different crystal structures, as shown in Table 1; for each size, we give the

Table 1. Relative Binding Energy of Mn at the Most Stable Sites for Different Sizes of ZnS Nanoplatelets with Respect to the Corresponding Wurtzite Phase

platelet size	ΔE_w (meV)	$\Delta E_{z\langle 110\rangle}$ (meV)	$\Delta E_{z\langle 111\rangle}$ (meV)
small	0	−40	−8
medium	0	−15	+11
bulk	0	+5	

results with respect to the wurtzite case. Table 1 shows that Mn incorporation lowers the energy the most for zinc blende nanoplatelets with the ⟨110⟩ orientation, representing a stability of 40 and 15 meV over the wurtzite phase for the small and the medium sized nanoplatelets, respectively. This reflects accurately the experimentally observed conversion of the undoped wurtzite nanoplatelet to the zinc blende ⟨110⟩ oriented nanoplatelets upon being doped by Mn; the strongest binding site for Mn in all of these cases is invariably found to be a subsurface site, in agreement with the EPR evidence.

Interestingly, the energy stability associated with the formation of the zinc blende structure upon Mn doping is obviously size-dependent, with the smallest sized nanoplatelet exhibiting the maximum stability of 40 meV over the wurtzite nanoplatelet. With an increase in the size to a 1.5 nm diameter platelet, the energy stability of the zinc blende phase over the wurtzite one decreases rapidly to 15 meV. While it proved impossible to carry out similar calculations for larger sized nanoplatelets due to computational limitations, we find that for a bulk ZnS system, Mn incorporation stabilizes the wurtzite structure, reversing the trend observed for the small nanoplatelets of ZnS. This systematic trend with the size is consistent with the experimental observation that the crystallographic phase transformation from the wurtzite to the zinc blende phase does not take place for large sized nanoplatelets. We have further carried out exploratory investigations on spherical nanoparticles of ZnS; our results indicate that Mn-doped ZnS in the zinc blende form is not stabilized over the wurtzite form for spherical nanoparticles, once again consistent with the experimental report.[8]

Encouraged by the above-mentioned close correspondence between experimental observations and our results in every aspect, we have attempted to obtain a microscopic understanding of this size-dependent doping-induced structural transition, driven apparently by certain size-dependent quantum confinement effects. We first analyze the bonding of Mn at the substitutional site by investigating Mn charge density along the Mn−S bond direction for various cases. We focus on changes in the charge density distribution in the zinc blende structure compared to the corresponding wurtzite charge density distribution. Figure 2a shows the results for the smallest nanoplatelets considered here. This figure shows that the charge density for the zinc blende case is substantially depleted near the Mn site, being pushed out toward the S site along the bond length compared to the wurtzite case. This clearly establishes a more covalent Mn−S bond in the zinc blende ⟨110⟩ nanoplatelet compared to that for the same sized wurtzite ⟨0001⟩ nanoplatelet. The larger sized nanoplatelets show a similar effect, though less pronounced compared to the case of the smaller sized nanoplatelet. Looking at the bulk case, we find that one has a reversal of the trend, with the charge density being more localized on the Mn in the zinc blende case, as shown in Figure 2b. Thus, the enhanced binding energy of Mn incorporation in the zinc blende ⟨110⟩ nanoplatelet (see Table 1), responsible for the structural transformation observed experimentally, is driven by a change in the covalency of the Mn−S bond in the two crystallographic forms as a function of the nanoplatelet size. The systematic enhancement of the covalency of the Mn−S bond for the zinc blende structure with

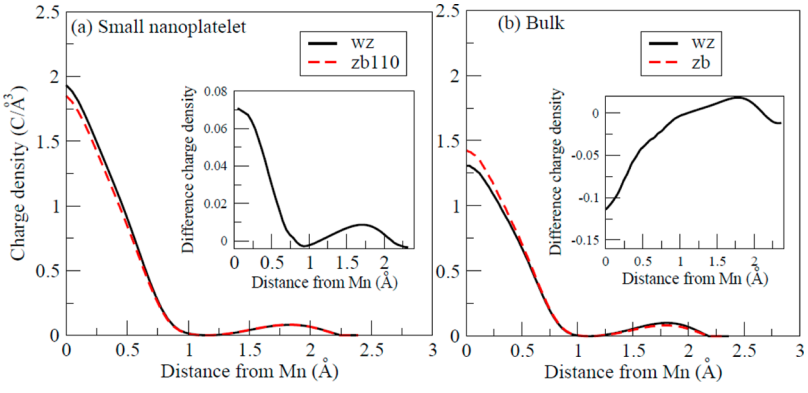

Figure 2. Charge density of Mn majority spin antibonding levels with t_2 symmetry for (a) wurtzite (0001) (wz) and zinc blende ⟨110⟩ (zb110) nanoplatelets and (b) wurtzite (wz) and zinc blende (zb) of bulk ZnS as a function of the distance from Mn along the Mn−S bond length. In the inset, the difference of the wz and zb charge density of the respective graph is shown. It should be noted that the charge conservation is not apparent in the figure, because the charge density is given only along the bond. Integrated charge density over the entire space is naturally conserved in all such calculations.

dx.doi.org/10.1021/jz4002746 | J. Phys. Chem. Lett. 2013, 4, 1023−1027

the decreasing size is responsible for the doped nanoplatelet favoring the zinc blende structure in the small size regime.

The covalency of any given bond is controlled by two parameters, namely, the energy difference and the hopping or the hybridization strength between the two orbitals participating in the bonding. The hybridization strength is a function of the interatomic distance or the bond length, the functional form depending on the nature of the orbitals involved. In this specific case, our calculations show that Mn−S bond lengths do not change perceptibly between the bulk and various nanoplatelets; consequently, we do not expect any significant change in the Mn d−S p hybridization strength. Therefore, the reversal of the Mn binding energy trend between the bulk and nanoplatelets shown in Table 1 cannot be associated with any change in the hopping strength leading to a change in the covalency. In order to understand the effect of the size on the remaining parameter, which is the energy difference between the Mn d and S p states, it is important to note here that Mn d levels, being essentially localized in nature, will not be affected significantly by the size of the cluster.[16−19] Therefore, we may consider the energy of Mn d levels to be practically constant for all cases considered here. In contrast, the S p levels are expected to be strongly influenced by the quantum confinement effect increasingly for smaller sized clusters.[20−23] We find direct evidence of this quantum confinement effect in the energy position of the VBM with dominantly S p character.

VBM referenced to the average electrostatic potential at the central Zn site for different cases are given in Table 2,

Table 2. Positions of VBM of Different Sizes of Nanoplatelets of ZnS As Well As That of Bulk ZnS[a]

platelet size	VBM-WZ⟨0001⟩ (eV)	VBM-ZB ⟨110⟩ (eV)	VBM-ZB⟨111⟩ (eV)
small	38.480	38.530	38.446
	(0.908)	(0.845)	(0.929)
medium	38.905	38.967	38.872
	(0.483)	(0.408)	(0.503)
bulk	39.388	39.375	
	(0.000)	(0.000)	

[a]The relative shifts of the VBM in the case of the wurtzite and zinc blende nanodisks with respect to the bulk values for the same structure are provided in parentheses.

exhibiting a pronounced dependence on the size for both crystallographic forms. Each type of system, be it wurtzite, zinc blende ⟨110⟩, or zinc blende ⟨111⟩, shows a systematic decrease of the energy of the VBM with a decrease in size. This can be ascribed to quantum confinement effects, as has already been observed for both the VBM and the conduction band minimum[20−23] for a wide variety of semiconductor materials. However, it is important to notice that the stabilization of the VBM compared to the bulk VBM, shown in brackets in Table 2, is more rapid for the wurtzite structure and the zinc blende nanoplatelet with ⟨111⟩ orientation compared to that for the zinc blende ⟨110⟩ oriented nanoplatelet. As a consequence, the VBM has the highest energy for the zinc blende ⟨110⟩ nanoplatelets (e.g., 38.530 eV for the small size) compared to those with the wurtzite structure (38.480 eV for the small size) and the zinc blende ⟨111⟩ one (38.446 eV for the small size) at any given size. Because the Mn d level lies above the VBM, a decreasing size implies that the energy separation between the two will increase more rapidly for the wurtzite and the zinc blende ⟨111⟩ nanoplatelets, making the Mn−S bond more ionic when compared to the relatively more covalently bonded Mn−S in the zinc blende ⟨110⟩ nanoplatelet due to the smallest Mn d−VBM energy separation in the latter. This is exactly what is reflected in the difference charge density plot in Figure 2, underlining the enhanced stability of Mn-doped zinc blende nanoplatelets with ⟨110⟩ orientation. Thus, we only need to understand the microscopic origin of the trend of quantum confinement effects on the position of the VBM given in Table 2, to obtain a complete understanding of the puzzling phenomenon.

In order to understand the origin of this more pronounced quantum confinement effect of the VBM for the wurtzite and zinc blende ⟨111⟩ nanoplatelets compared to that of the zinc blende ⟨110⟩ nanoplatelets, we first note that the shift in energies in such confined systems is inversely related to the relevant effective hole mass. Thus, we have computed the effective hole mass in several directions for the bulk zinc blende and wurtzite unit cells. However, the confinement in nanoplatelets is primarily determined by the effective hole mass in the growth direction because we have just four monolayers in thickness defining the smallest dimension in the problem. The effective hole masses along the ⟨0001⟩ direction in the wurtzite structure and those along the ⟨111⟩ and ⟨110⟩ directions in the zinc blende structure are 1.2, 1.5, and 3.5 m_e, respectively. As the hole effective mass (1.2 m_e) for wurtzite along the ⟨0001⟩ direction and that (1.5 m_e) for the zinc blende along the ⟨111⟩ direction are smaller than that (3.5 m_e) for zinc blende in the ⟨110⟩ direction; the VBMs get pushed down more rapidly for the wurtzite and the zinc blende ⟨111⟩ cases compared to that for the zinc blende ⟨110⟩ case, providing the final microscopic explanation of the observed unusual structural transition in ZnS nanoplatelets induced by Mn doping.

Thus, it appears that differences in the relevant effective masses in the bulk semiconductor control the Mn-dopant-induced crystal structure transformation in ZnS nanoplatelets via quantum confinement effects. This fact, though rarely appreciated in the past, must be operational in a large number of other contexts, besides such structural transformations, because changing covalency of chemical bonds influences a wide range of chemical properties.

AUTHOR INFORMATION

Corresponding Author

*E-mail: priya@bose.res.in (P.M.); sarma@sscu.iisc.ernet.in (D.D.S.).

Author Contributions

[§]C.G. and R.D. have contributed equally.

Notes

The authors declare no competing financial interest.

ACKNOWLEDGMENTS

The authors thank the Department of Science and Technology, India. D.D.S. and R.D. thank the Council of Scientific and Industrial Research, India. We thank Saikat Debnath for helping us with the figures.

REFERENCES

(1) Ito, T. Simple Criterion for Wurtzite−Zinc-Blende Polytypism in Semiconductors. *Jpn. J. Appl. Phys.* **1998**, *37*, L1217−L1220.

(2) Yeh, C. -Y.; Lu, Z. W.; Froyen, S.; Zunger, A. Predictions and Systematizations of the Zinc-Blende−Wurtzite Structural Energies in Binary Octet Compounds. *Phys. Rev. B* **1992**, *45*, 12130−12133.
(3) Mujica, A.; Rubio, A.; Muñoz, A.; Needs, R. J. High-Pressure Phases of Group-IV, III−V, and II−VI Compounds. *Rev. Mod. Phys.* **2003**, *75*, 863−912.
(4) Kruszynska, M.; Borchert, H.; Parisi, J.; Kolny-Olesiak, J. Synthesis and Shape Control of $CuInS_2$ Nanoparticles. *J. Am. Chem. Soc.* **2010**, *132*, 15976−15986.
(5) Nag, A.; Hazarika, A.; Shanavas, K. V.; Sharma, S. M.; Dasgupta, I.; Sarma, D. D. Crystal Structure Engineering by Fine-Tuning the Surface Energy: The Case of CdE (E = S/Se) Nanocrystals. *J. Phys. Chem. Lett.* **2011**, *2*, 706−712.
(6) Huang, J.; Kovalenko, M. V.; Talapin, D. V. Alkyl Chains of Surface Ligands Affect Polytypism of CdSe Nanocrystals and Play an Important Role in the Synthesis of Anisotropic Nanoheterostructures. *J. Am. Chem. Soc.* **2010**, *132*, 15866−15868.
(7) Polking, M. J.; Urban, J. J.; Milliron, D. J.; Zheng, H.; Chan, E.; Caldwell, M. A.; Raoux, S.; Kisielowski, C. F.; Ager, J. W., III; Ramesh, R.; Alivisatos, A. P. Size-Dependent Polar Ordering in Colloidal GeTe Nanocrystals. *Nano Lett.* **2011**, *11*, 1147−1152.
(8) Karan, N. S.; Sarkar, S.; Sarma, D. D.; Kundu, P.; Ravishankar, N.; Pradhan, N. Thermally Controlled Cyclic Insertion/Ejection of Dopant Ions and Reversible Zinc Blende/Wurtzite Phase Changes in ZnS Nanostructures. *J. Am. Chem. Soc.* **2011**, *133*, 1666−1669.
(9) Takahashi, K.; Morizumi, T. Growth of InAs Whiskers in Wurtzite Structure. *Jpn. J. Appl. Phys.* **1998**, *5*, L1217−L1220.
(10) Dalpian, G. M.; Wei, S.-H. Hole-Mediated Stabilization of Cubic GaN. *Phys. Rev. Lett.* **2004**, *93*, 216401.
(11) Choi, E.-A.; Kang, J.; Chang, K. J. Energetics of Cubic and Hexagonal Phases in Mn-Doped GaN: First-Principles Pseudopotential Calculations. *Phys. Rev. B* **2006**, *74*, 245218.
(12) Bergerhoff, G.; Brown, I. D. *Crystallographic Databases*; Allen, F. H., Bergerhoff, G., Sievers, R., Eds.; International Union of Crystallography: Chester, U.K.; 1987.
(13) Kresse, G.; Joubert, D. From Ultrasoft Pseudopotentials to the Projector Augmented-Wave Method. *Phys. Rev. B* **1999**, *59*, 1758−1775.
(14) Kresse, G.; Furthmüller, J. Efficient Iterative Schemes for *Ab Initio* Total-Energy Calculations Using a Plane-Wave Basis Set. *Phys. Rev. B* **1996**, *54*, 11169−11186.
(15) Perdew, J. P.; Zunger, A. Self-Interaction Correction to Density-Functional Approximations for Many-Electron Systems. *Phys. Rev. B* **1981**, *23*, 5048−5076.
(16) Cherian, R.; Mahadevan, P. Bulk and Nanoscale GaN: Role of Ga d States. *Phys. Rev. B* **2007**, *76*, 075205.
(17) Caldas, M. J.; Fazzio, A.; Zunger, A. A Universal Trend in the Binding Energies of Deep Impurities in Semiconductors. *Appl. Phys. Lett.* **1984**, *45*, 671−673.
(18) Huang, X.; Makmal, A.; Chelikowsky, J. R.; Kronik, L. Size-Dependent Spintronic Properties of Dilute Magnetic Semiconductor Nanocrystals. *Phys. Rev. Lett.* **2005**, *94*, 236801.
(19) Norberg, N. S.; Dalpian, G. M.; Chelikowsky, J. R.; Gamelin, D. R. Energetic Pinning of Magnetic Impurity Levels in Quantum-Confined Semiconductors. *Nano Lett.* **2006**, *6*, 2887−2892.
(20) Sapra, S.; Sarma, D. D. Evolution of the Electronic Structure with Size in II−VI Semiconductor Nanocrystals. *Phys. Rev. B* **2004**, *69*, 125304.
(21) Sapra, S.; Shanthi, N.; Sarma, D. D. Realistic Tight Binding Model for the Electronic Structure of II−VI Semiconductors. *Phys. Rev. B* **2002**, *66*, 205202.
(22) Viswanatha, R.; Sapra, S.; Saha-Dasgupta, T.; Sarma, D. D. Electronic Structure of and Quantum Size Effect in III−V and II−VI Semiconducting Nanocrystals Using a Realistic Tight Binding Approach. *Phys. Rev. B* **2005**, *72*, 045333.
(23) Viswanatha, R.; Sarma, D. D. Effect of Structural Modification on the Quantum-Size Effect in II−VI Semiconducting Nanocrystals. *Chem. Asian J.* **2009**, *4*, 904−909.